Supporting Information

Dehydroxylation Driven Reactivity in Kaolinite: Unraveling Strain Structure Interplay for Enhanced Electrocatalytic Water Splitting

Jeygeerthika Reddy [a], Meyyappan Chidambaram Karuppaiah Shankar [a], K.K.Viswanathan[b] , Kunmo Koo [c], Prabakar Kandasamy [a#]

[a]Advanced Sustainable Energy Laboratory, Department of Electrical and Electronics Engineering, Pusan National University, Busan, South Korea.

[b]Department of Mathematical Modeling, Faculty of Mathematics, Samarkand State University, Samarkand, 140104, Uzbekistan.

[c] School of Materials Science and Engineering, Pusan National University, Busan 46241, Republic of Korea.

[d] Institute of Materials Technology, Pusan National University, Busan 46241, Republic of Korea.

[#]Corresponding author

E-mail: prabakar@pusan.ac.kr

Characterizations

The surface morphology of the catalysts was analyzed using field-emission scanning electron microscopy (FESEM, Zeiss SUPRA 25). The crystal- line structure of the materials was identified using an X-ray diffractometer (XRD, XPERT-PRO) operating at a generator voltage of 40 kV and tube current of 30 mA with monochromatic Cu-Kα radiation in the 2θ range from 10-80◦. Fourier Transform Infrared Spectroscopy (FTIR) was studied at Pusan National University lab-center (IS50 instrument). TEM samples were analyzed by Cs Corrected Transmission Electron Microscope (JEM-ARM200F), Core Research Facilities (CRF) at Pusan National University. Thermogravimetric analysis (TGA) was analyzed at KIST institute (TGA55 instrument). Elemental compositions and surface oxidation states of the catalysts were studied by using angle-resolved X-ray photoelectron spectroscopy (AR-XPS, Thermo Fisher Scientific (U.K.)) with monochromatic Al-Kα radiation of 1486.6 eV in KBSI Busan. XPS peak fitting was done by using CASA XPS software. Electron paramagnetic resonance (EPR) measurements were carried out at the Korea Basic Science Institute (KBSI), Seoul, Korea, using a Bruker EMXplus spectrometer. X-band (≈9 GHz) continuous-wave (CW) EPR spectra were recorded at room temperature.

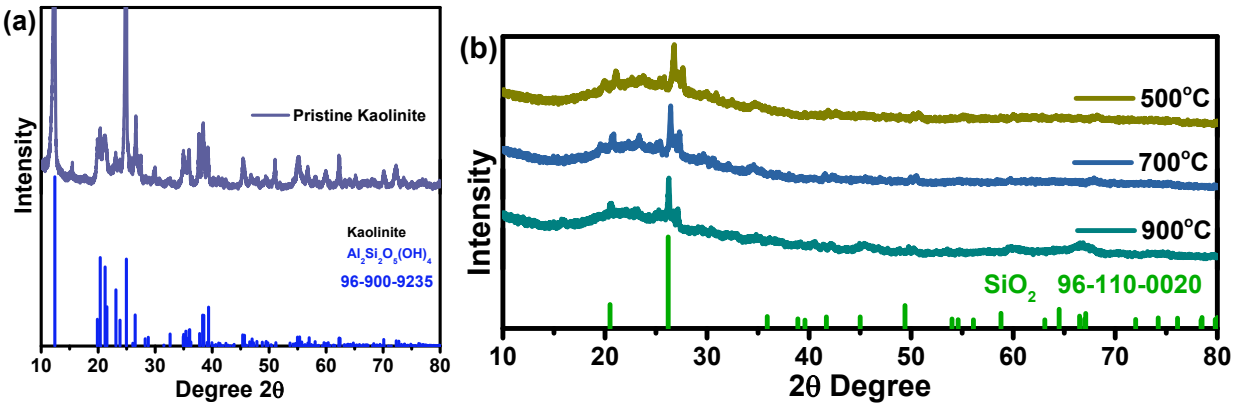

Figure S1: (a) XRD patterns of pristine sample. (b) XRD pattern of annealed sample.

Methods & formula of XRD (For table 1)

- **Scherrer method (crystallite size)**

$$D_{Scherrer} = \frac{k\lambda}{\beta cos\theta}$$

where k(shape factor) ≈ 0.9, λ is X-ray wavelength, β is the FWHM (radians) corrected for instrumental broadening, and θ is the Bragg angle. Scherrer gives the *coherent diffraction domain* size; it assumes broadening is due to finite size only (no strain).

- **Williamson–Hall (W–H) method (separates size & strain)**

The W–H linear form:
$$\beta cos\theta = \frac{k\lambda}{D_{W-H}} + 4\varepsilon sin\theta$$

Intercept → $k\lambda/D_{W-H}$ size contribution). Slope → ε (microstrain, ε). W–H therefore gives a size corrected for the contribution of lattice strain.

- **Dislocation density (approx.)**

A commonly used estimate: $\rho \approx \frac{1}{D^2}$ ρ≈1/D2 (with D in metres).

If D is in nm, $\rho = 10^{18}/D^2$ (units m^{-2}).

- **Sign of strain**

By convention that (-ve) value indicates a net *compressive microstrain* (lattice contraction) in the crystallites vs. the reference lattice. The sign depends on how the peak shifts/broadens were fitted; negative values are valid and physically meaningful (net lattice contraction / compressive distortions).

Table S1: Average structural parameters of all the samples.

Sample	Scherrers method		W-H Method	
	D(nm)	Dislocation lines	D (nm)	Strain
Pristine Kaolinite	11.60	7.42 x 10^{15}	10.24	-0.00118
KAO@100	11.24	7.91 x 10^{15}	9.65	-0.001
KAO@300	12.12	6.81 x 10^{15}	10.19	-0.001130
KAO@500	7.92	15.9 x 10^{15}	4.33	-0.00859
KAO@700	8.72	13.1 x 10^{15}	3.8	-0.01103
KAO@900	7.56	17.5 x 10^{15}	5.77	-0.00316

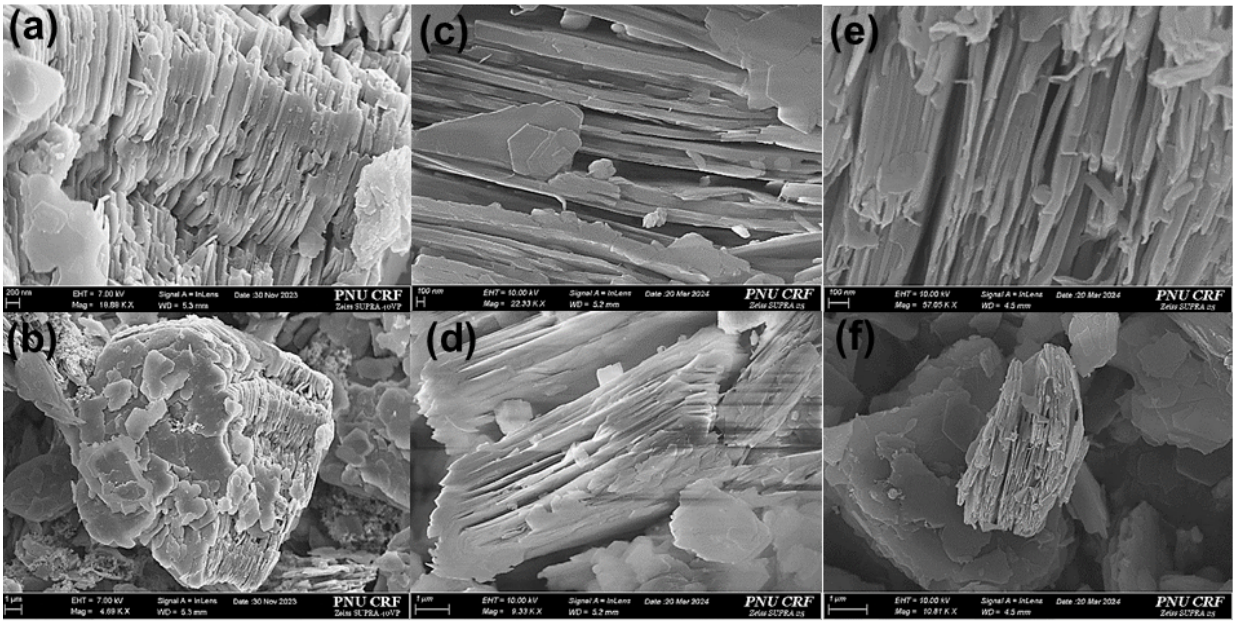
(a)
(c)
(e)
(b)
(d)
(f)
PNU CRF

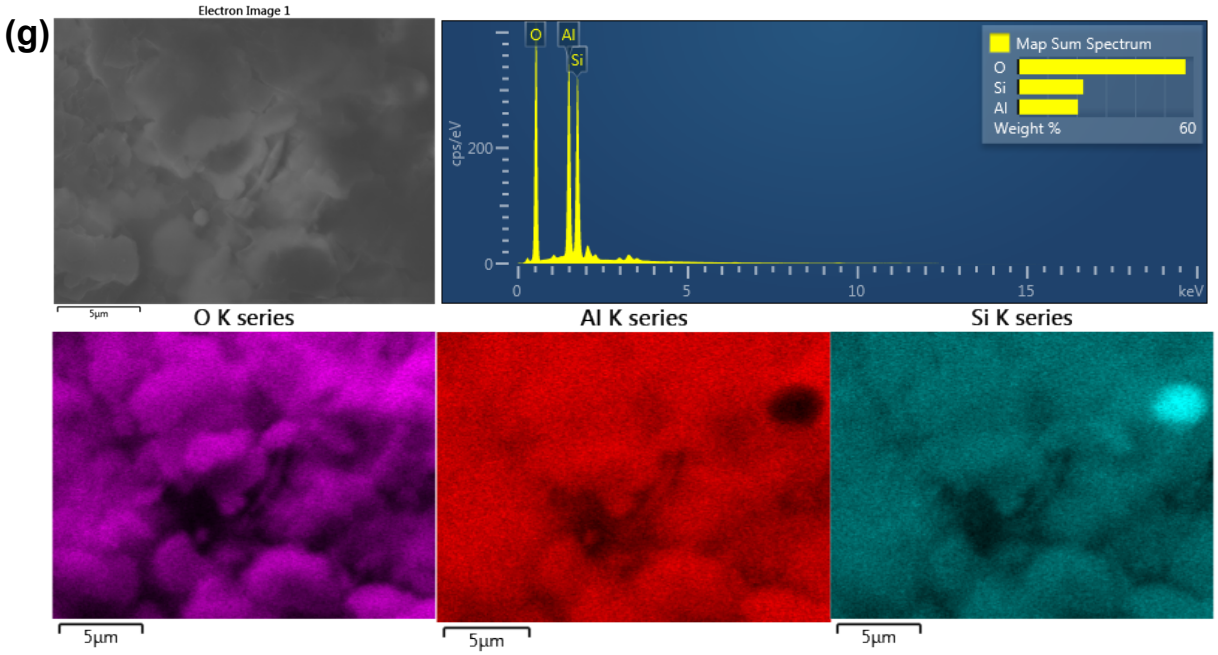
(g)
Electron Image 1
5µm
O
Al
Si
cps/eV
200
0
0
5
10
15
keV
Map Sum Spectrum
O
Si
Al
Weight %
60
O K series
Al K series
Si K series
5µm
5µm
5µm

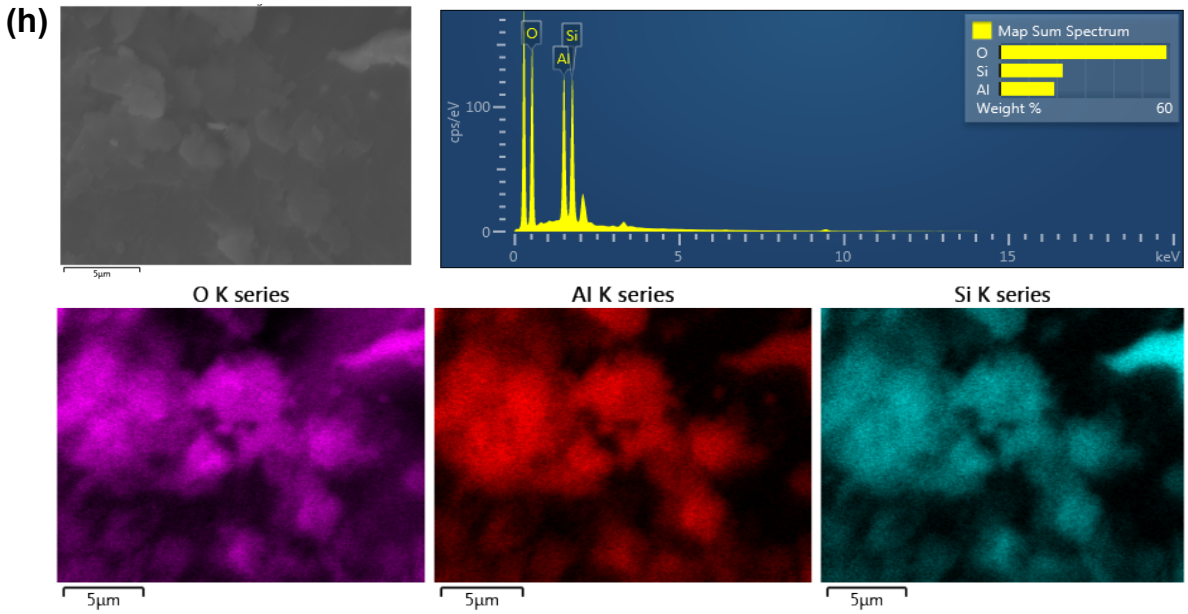

Figure S2: FE-SEM images of powder samples (a-b) pristine Kaolinite, (c-d) KAO@100, (e-f) KAO@900. EDAX spectra and elemental images of samples (g) KAO@100 and (h) KAO@900.

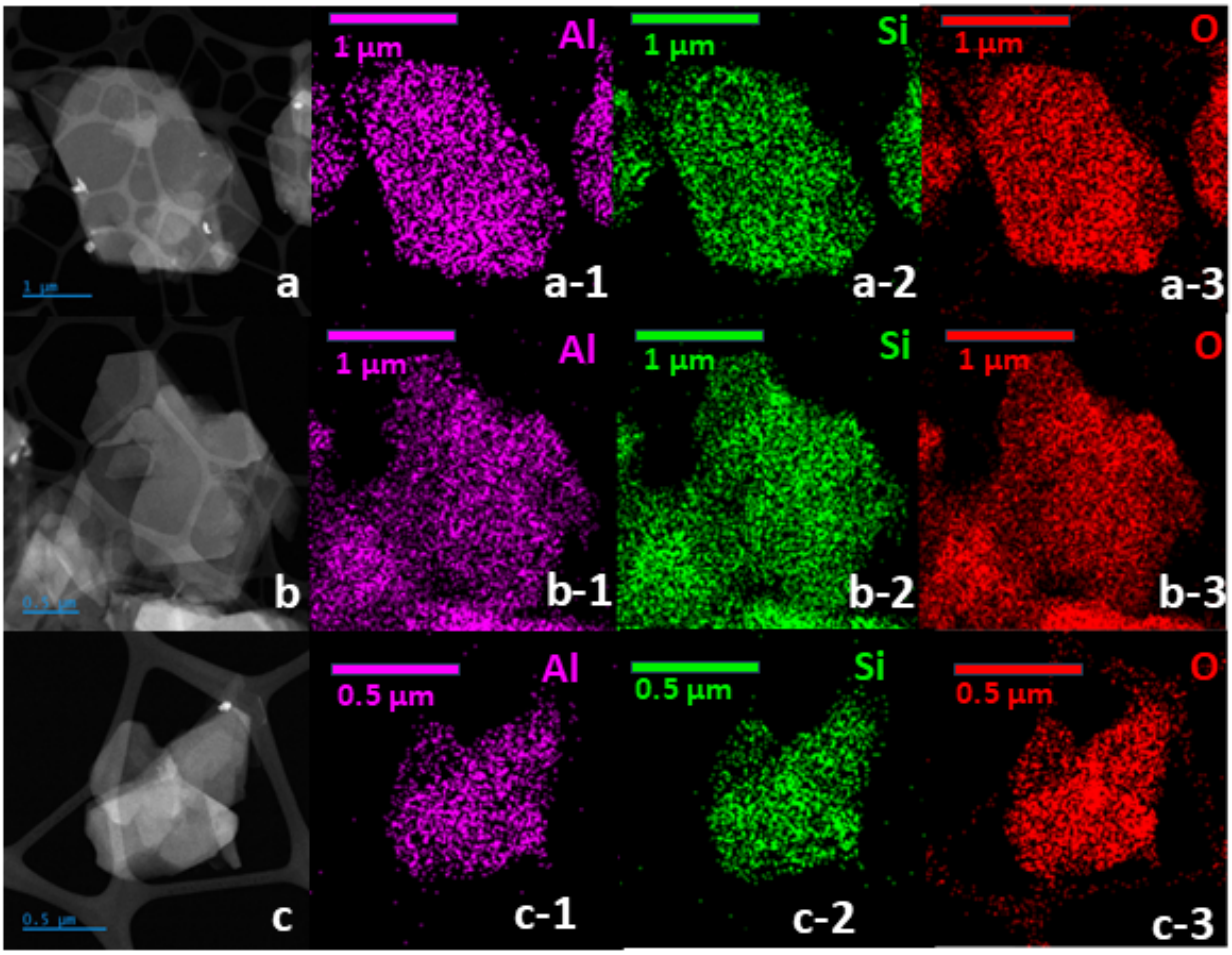

Figure S3: FE-TEM images, HAADF and EDX mapping, of (a) Pristine Kaolinite, (b) KAO@100, (c) KAO@900.

Table S2: Detailed interpretation of XPS Spectra.

Sample	Element	Peak Position (eV)	Assigned Component	Area % of components
100 °C	Al 2p	74.33	Al–O (Octahedral)	78.39
	Al 2p	75.11	Al–OH / Distorted Al	21.61
	O 1s	531.00	Lattice O^{2-}	30.62
	O 1s	532.43	Surface –OH	44.94
	O 1s	533.29	Adsorbed H_2O / Defects	24.43
	Si 2p	102.78	Si–O–Si / Si–O–Al	100
700 °C	Al 2p	74.38	Reorganized Al–O	76.24
	Al 2p	75.24	Residual Al–OH	23.76
	O 1s	531.97	Lattice O^{2-} (activated)	61.97
	O 1s	532.85	Surface O species	33.25
	O 1s	533.85	Weakly bound oxygen	4.78
	Si 2p	102.63	Si–O network	100
900 °C	Al 2p	74.38	Metakaolinite Al–O	100
	O 1s	532.13	Lattice O^{2-}	59.19
	O 1s	532.85	Stable surface oxygen	40.81
	Si 2p	102.69	Reorganized Si–O	100

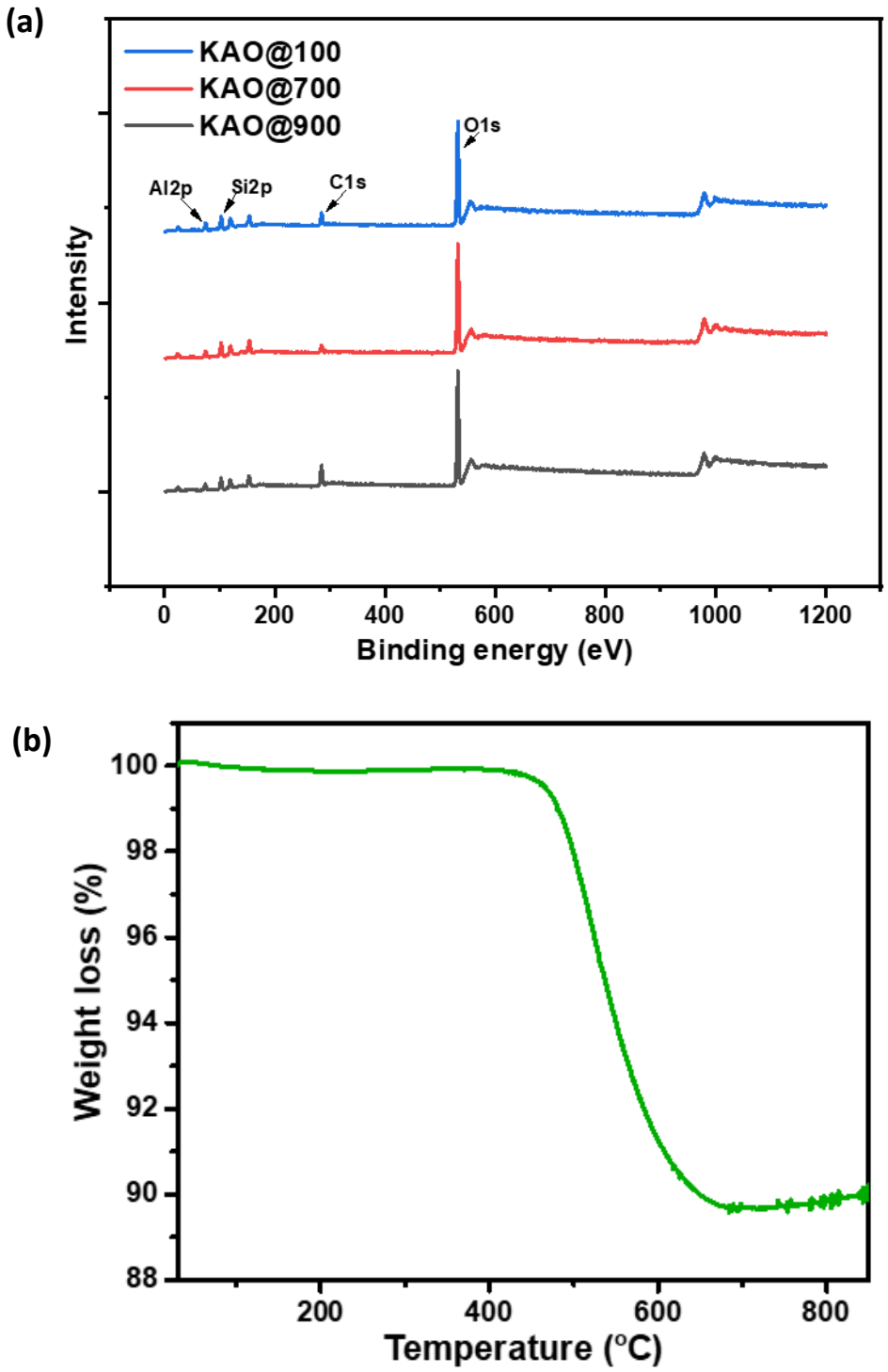

Figure S4: (a) XPS survey spectrum, (b) Thermogravimetric Analysis of Kaolinite.

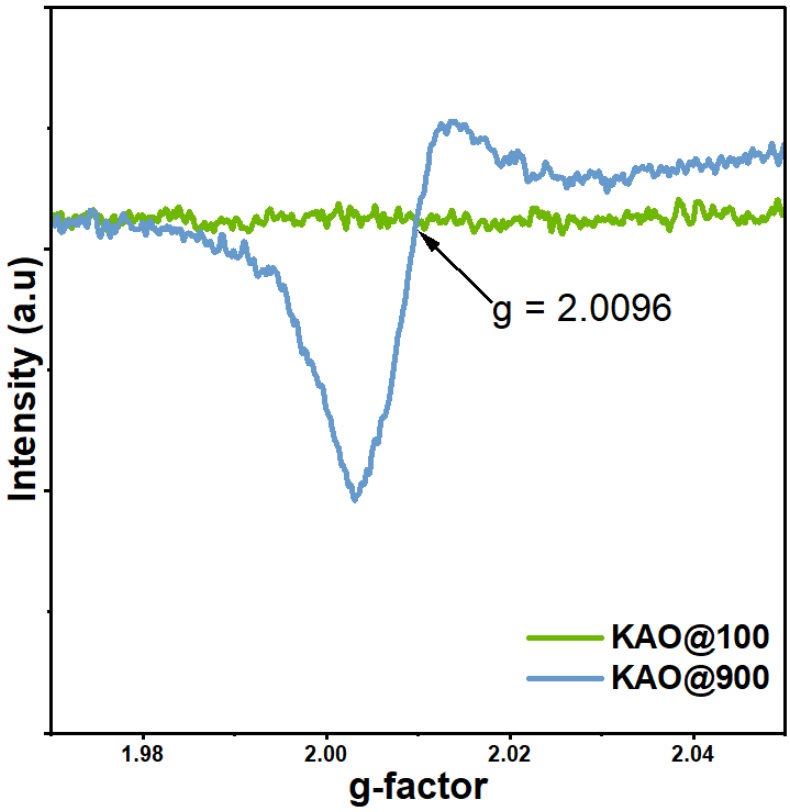

Figure S5: EPR of KAO@100 and KAO@900 samples.

The EPR spectra of Kao@100 and Kao@900 samples are shown in Fig. S5. The Kao@100 sample exhibits a nearly flat signal with very low intensity, indicating the absence or negligible presence of unpaired electrons or defect centers. This suggests that the structure is relatively defect-free. In contrast, the Kao@900 sample displays a prominent EPR signal centered at a g-factor of 2.0096, which is characteristic of oxygen vacancy–related defect sites. The appearance of this distinct resonance signal indicates the generation of unpaired electrons associated with oxygen-deficient centers confirming that high-temperature treatment induces defect formation in the kaolinite structure. The increased signal intensity further reflects a higher concentration of these paramagnetic centers. Overall, the EPR results clearly demonstrate that thermal treatment at 900°C

leads to the formation of oxygen vacancies and defect sites, which can play a crucial role in enhancing the catalytic activity of the material.

Electrochemical measurements

The electrochemical measurements were conducted in a three-electrode cell setup using a Biologic SP-150 electrochemical workstation in a 1 M KOH solution. A Hg/HgO (1 M KOH saturated) electrode was used as the reference electrode, a graphite rod as the counter electrode, and the slurry-coated Kaolinite/NF material served as the working electrode. Prior to starting the electrochemical experiments, the electrolyte solution was purged with high-purity N_2 gas (99.999%) for 30 minutes to remove any dissolved oxygen ions. The measured potential with respect to the Hg/HgO reference electrode ($E_{Hg/HgO}$) was then converted to the standard reversible hydrogen electrode (E_{RHE}) using the Nernst equation provided

$$E_{RHE} = E_{Hg/HgO} + 0.098 + 0.059 \times pH \qquad (1)$$

Here, the pH value of 1 M KOH solution was 14. Polarization curves reported here are corrected with 85% instrument-supported iR correction to avoid the effect of solvent resistance. Here, i is the measured current and R is the uncompensated resistance between reference and working electrodes. The OER over- potential (η) was estimated using the equation as follows

$$\eta = E_{RHE} - 1.23 \qquad (2)$$

Electrochemical active surface area (ECSA) of catalyst is directly proportioning to the double-layer capacitance (Cdl) value. Cdl was derived from the below equation.

$$\Delta j = 2.\nu.C_{dl} \qquad (3)$$

where Δj is difference in anodic and cathodic current density and ν is scan rate. To calculate turn-over frequency (TOF), the concentration of surface- active sites or electrochemically accessible active sites were measured from the reduction region of CV at a scan rate of 50 mVs^{-1}.

$$C = \frac{\int area\ of\ reduction\ peak/scan\ rate}{Charge\ of\ one\ elctron} \quad (4)$$

$$TOF = j.\frac{NA}{n.F.C}s^{-1} \quad (5)$$

where j = measured current density, NA = Avogadro's number, n = number of electrons transferred (n = 4 is for OER), F = Faraday constant and C = concentration of surface-active sites. The durability test of the catalyst was studied by the chronopotentiometry technique (CP) at a constant current density of 100 mA cm^{-2}. Chronoamperometry test was taken at different potentials to study the catalysts behavior in steady state condition.

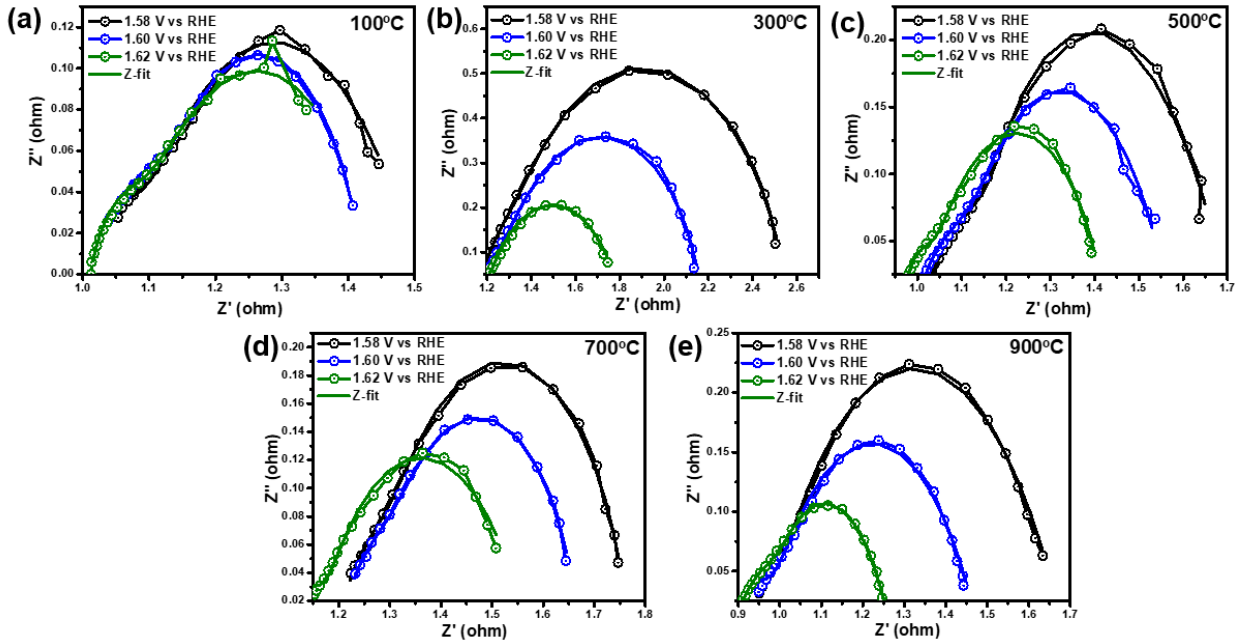

Figure S6: (a-e) Nyquist plots at different OER potentials, (f) Equivalent circuit for Nyquist plot fitting.

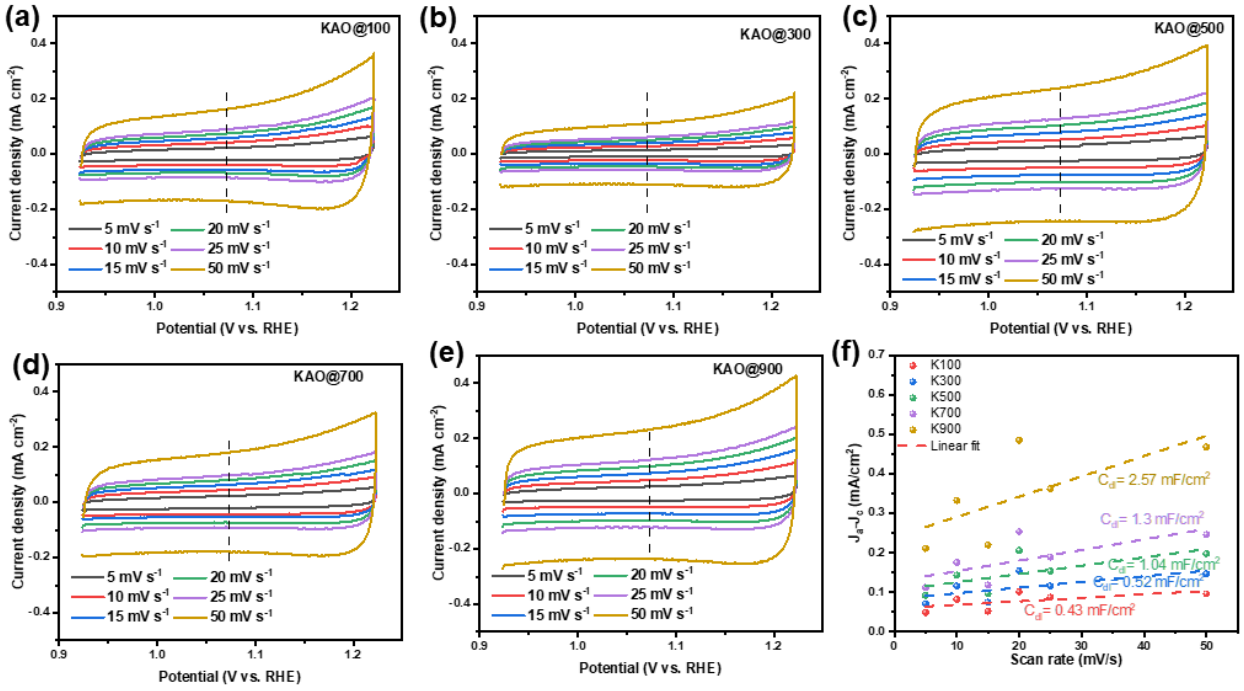

Figure S7: (a-e) CV curves in faradic potential range for the estimation of Cdl (f) ΔJ vs Scan rate plot.

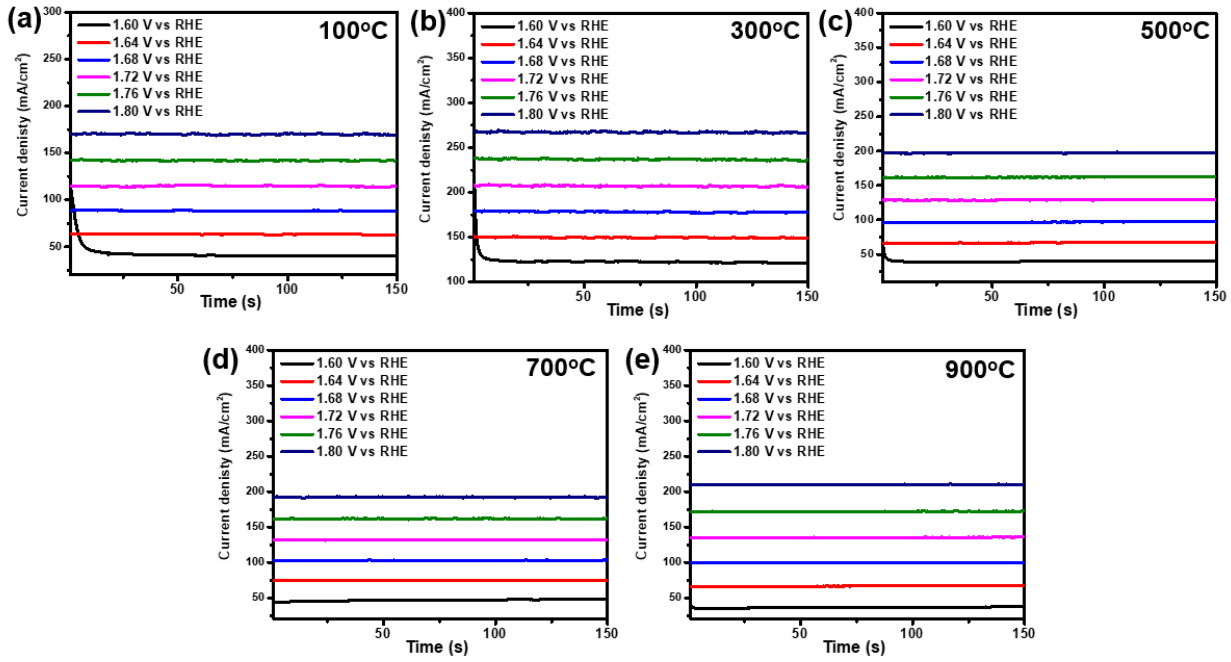

Figure S8: Chronoamperometry plots at different OER potentials

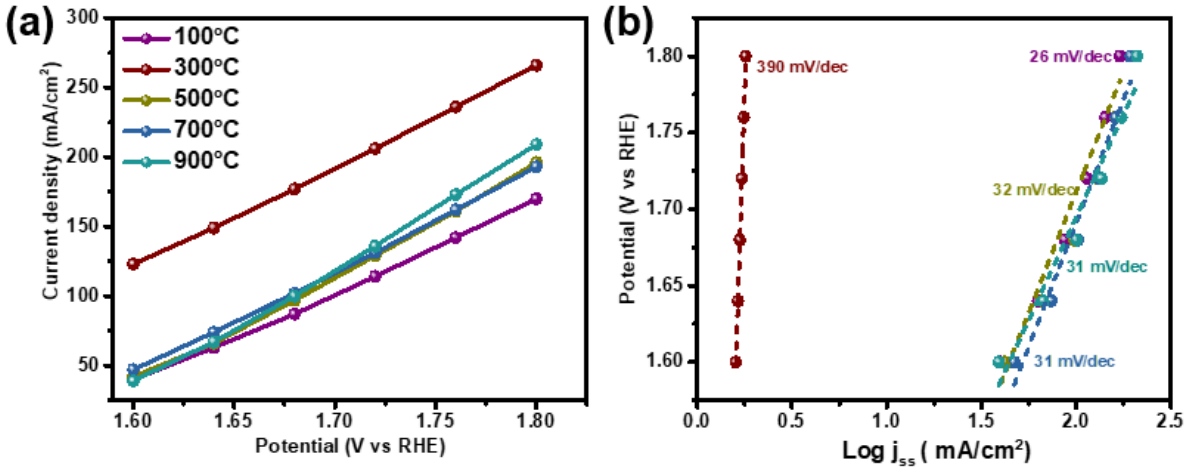

Figure S9: (a) Polarization curve from CA method at OER current densities, (b) Corresponding Tafel slope.

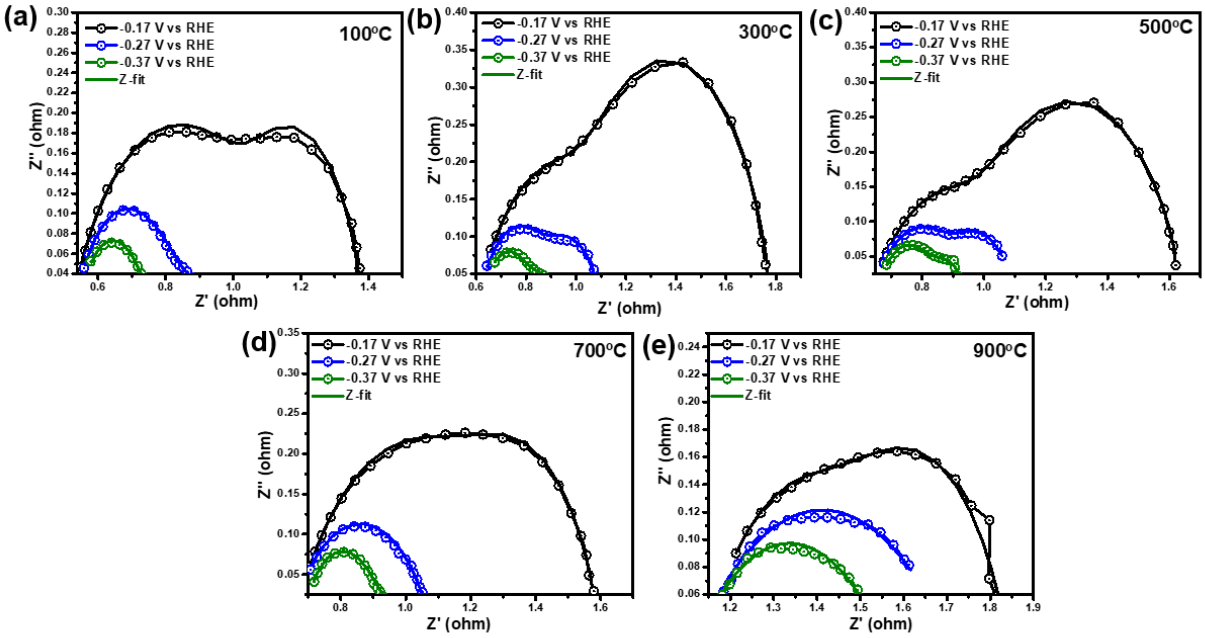

Figure S10: Nyquist plots at different HER potentials

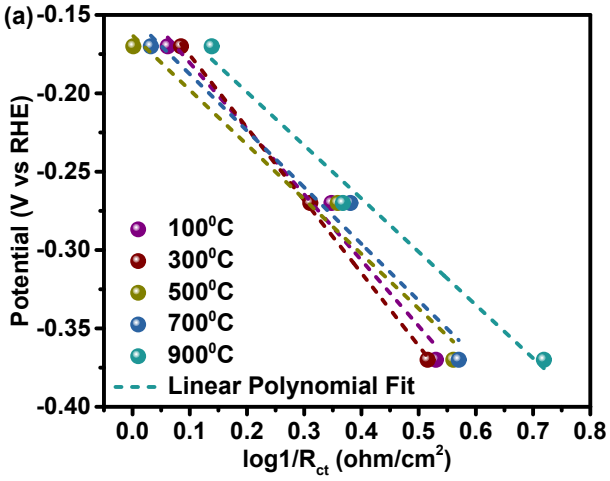

Figure S11: V vs log($1/R_{ct}$) plot from Nyquist plot.

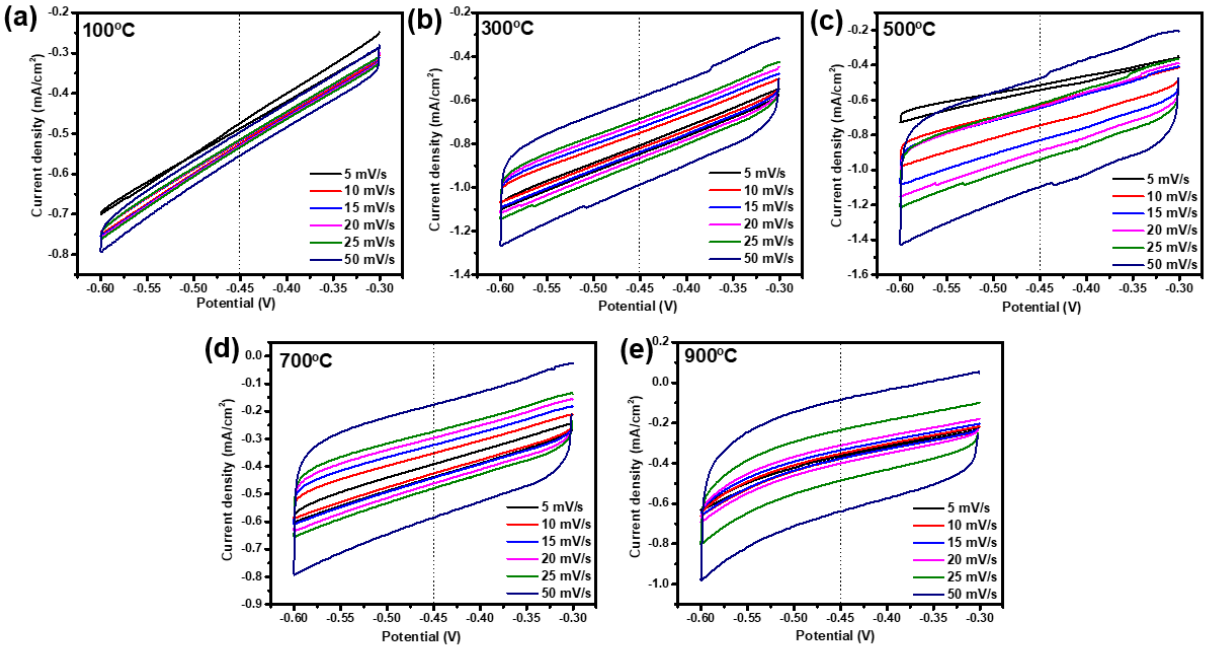

Figure S12: CV curves in non-faradic potential range for the estimation of Cdl

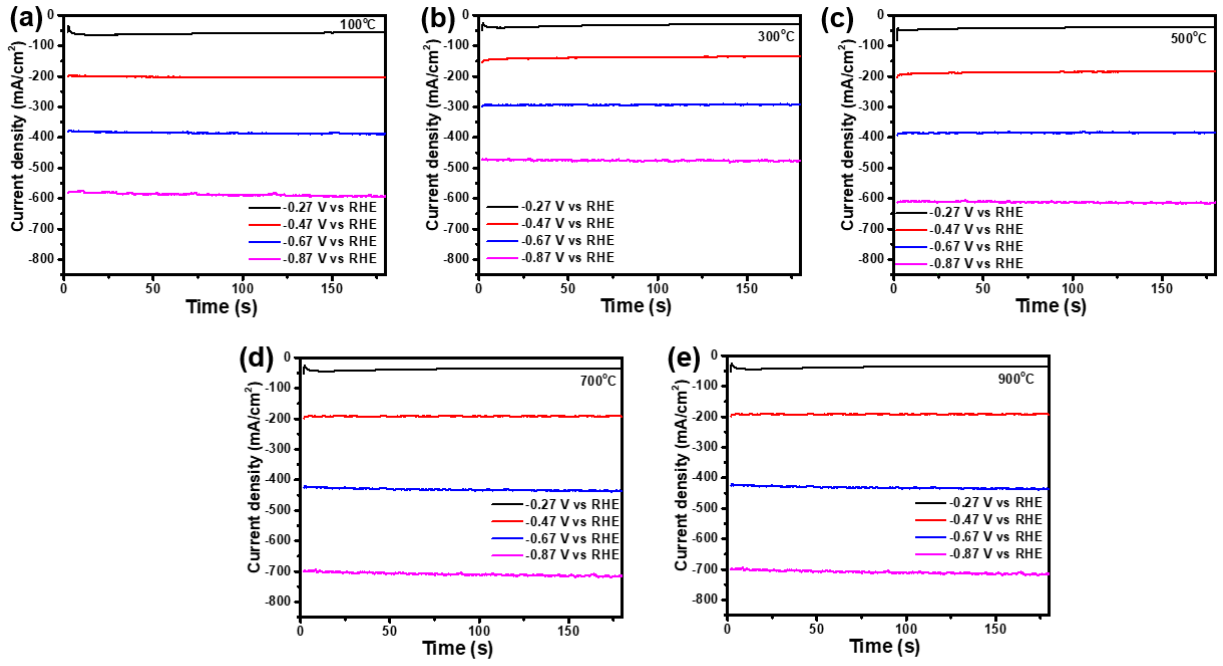

Figure S13: Chronoamperometry plots at different HER potentials

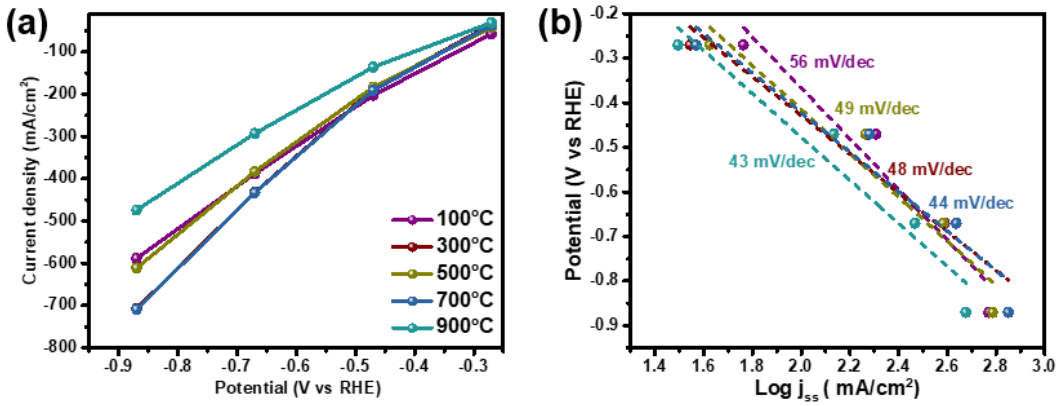

Figure S14: (a) Polarization curve from CA method at HER current densities, (b) Corresponding Tafel slope.

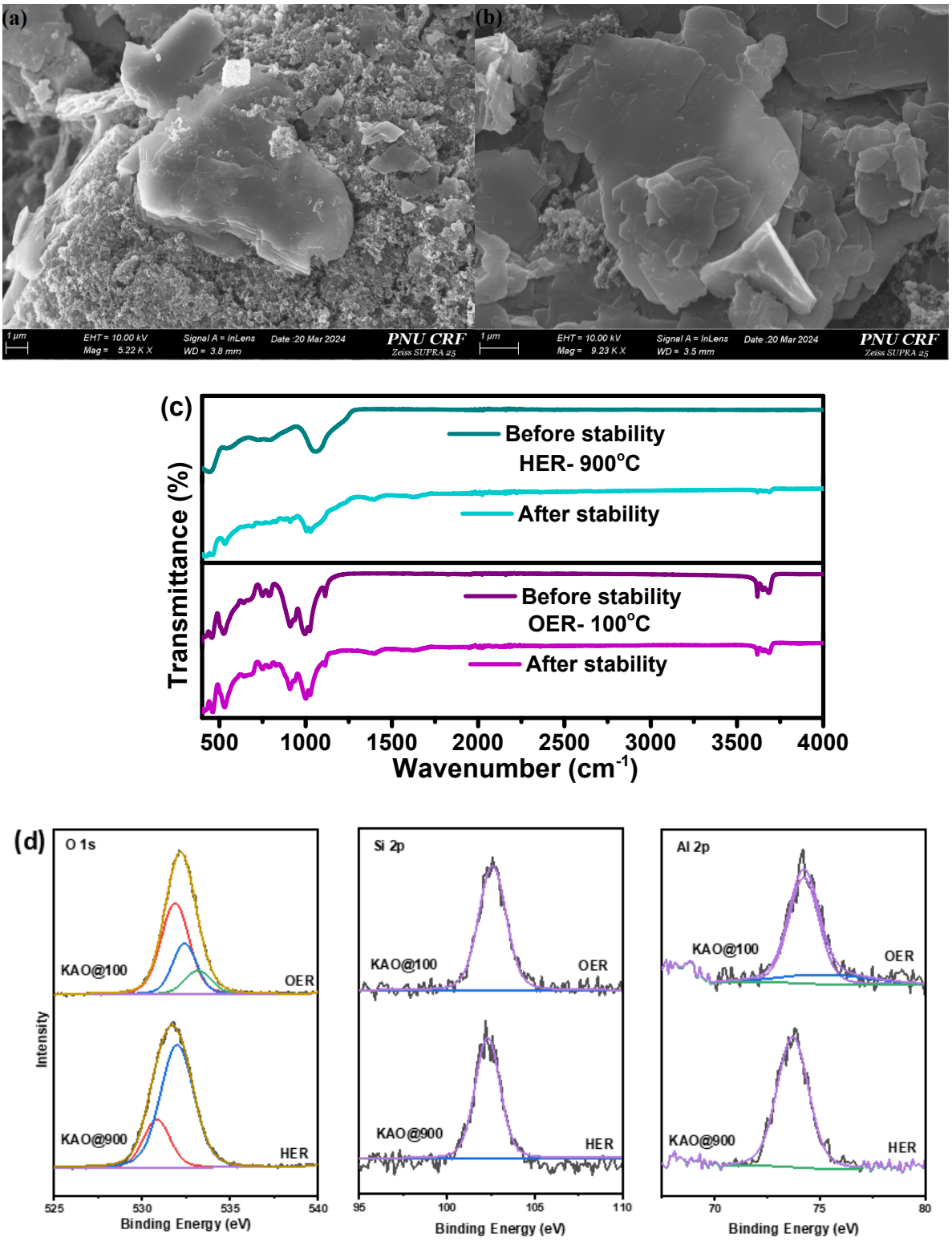

Figure S15: SEM images of after the stability studies (a) 900^{o} C, (b) 100^{0} C kaolinite. (c) FTIR and (d) XPS spectra